Fibers and Polymers 2018, Vol.19, No.3, 561-570
DOI 10.1007/s12221-018-7699-9

ISSN 1229-9197 (print version)
ISSN 1875-0052 (electronic version)

Effects of Chemical Functionalization of MWCNTs on the Structural and Physical Properties of Elastomeric Copolyetherester-based Composite Fibers

Min Ho Jee and Doo Hyun Baik*

Department of Advanced Organic Materials and Textile System Engineering, Chungnam National University, Daejeon 34134, Korea

(Received November 1, 2017; Revised January 11, 2018; Accepted January 28, 2018)

Abstract: Elastomeric copolyetherester (CPEE)-based composite fibers incorporating various neat and functionalized multi-walled carbon nanotubes (MWCNTs) were prepared through a conventional wet-spinning and coagulation process. The influence of functionalized MWCNTs on the morphological features, and the thermal, mechanical properties and electrical conductivity of CPEE/MWCNT (80/20, w/w) composite fibers were investigated. FE-SEM images show that a composite fiber containing poly(ethylene glycol)-functionalized MWCNTs (MWCNT-PEG) has a relatively smooth surface owing to the good dispersion of MWCNT-PEGs within the fiber, whereas composite fibers including pristine MWCNTs (p-MWCNT), acid-functionalized MWCNTs (a-MWCNT), and ethylene glycol-modified MWCNTs (MWCNT-EG) have quite a rough surface morphology owing to the presence of MWCNT aggregates. As a result, the CPEE/MWCNT-PEG composite fiber exhibits noticeably increased thermal and tensile mechanical properties as well as a faster crystallization behavior, which stems from an enhanced interfacial interaction between the CPEE matrix and MWCNT-PEGs.

Keywords: Functionalized MWCNTs, Composite fibers, Wet-spinning, Morphological features, Mechanical property

Introduction

As a new class of composite fiber materials, polymer composite fibers that include carbon nanotubes (CNTs) have attracted significant attention from the industry and academia owing to the excellent mechanical, thermal, and electrical properties of the CNTs [1-11]. In particular, the unique properties of CNTs provide the opportunity to make much stronger and more functional composite fibers than currently used polymeric fibers such as polyester, nylon, polyethylene, acrylic, Kevlar®, and Zylon® [12].

A wide range of studies using conventional melt-, wet- and dry-spinning methods have progressed the manufacturing of CNT-incorporated polymer composite fibers [13-21], including polymeric materials such as poly(ethylene terephthalate) (PET), poly(vinyl alcohol) (PVA), poly(p-phenylene benzobisoxazole) (PBO), and polyacrylonitrile (PAN). Shen *et al.* prepared PET/CNT composite fibers using a conventional melt-spinning method [22], and found that the tensile strength and initial modulus of the composite fiber were increased by 36.9 % and 41.2 % when using 0.2 wt% acid-treated MWCNTs, respectively, compared with neat PET fibers. Kumar *et al*. described the possibility of manufacturing super-strong composite fibers using the dry-jet wet spinning of PBO/SWCNT [23]. The authors reported that the tensile modulus and tensile strength of PBO-based composite fibers containing 10 wt% SWCNTs were increased by 61.5 % and 21.0 %, respectively, compared with heat-treated PBO fibers (Zylon® HM). In particular, the compressive strength of the PBO/SWCNTs composite fibers was measured to be 0.50 GPa, which is 43 % higher than that (0.35 GPa) of neat PBO fibers. This result demonstrates that the addition of CNTs can improve the compressive strength of composite fibers as a good reinforcing material, in addition to its tensile strength and modulus. The researchers also suggested that PAN/SWCNT composite fibers manufactured through a gel-spinning method could be used as a precursor for carbon fibers with improved mechanical properties. They reported that carbonized PAN/SWCNT composite fibers exhibit a higher orientation, smaller graphite *d*-spacing, larger crystal size, and improved tensile mechanical properties, in comparison to carbonized PAN fibers prepared under similar conditions [24,25].

Meanwhile, Vigolo *et al*. reported SWCNT/PVA composite fibers prepared using a unique combination of wet spinning and coagulation [26,27]. Composite fibers containing up to ~60 wt% SWCNTs have an elastic modulus ten-times higher than that of high-quality SWCNT bucky paper, and thus can be tied into knots without breaking, unlike classical carbon fibers. Furthermore, Dalton *et al*. found that the alignment of CNTs in the SWCNT/PVA composite fibers play a major role in the highly improved mechanical properties of the composite fibers [28,29]. We also recently prepared MWCNT/PVA composite fibers using wet spinning and coagulation [30,31]. It was revealed that the mechanical and electrical properties of the MWCNT/PVA composite fibers could be strongly affected by the alignment of MWCNTs within the fibers.

As described above, the structures and properties of polymer/CNT composite fibers are highly dependent on the

*Corresponding author: dhbaik@cnu.ac.kr

amount, alignment, and dispersion of the CNTs, and on the specific interfacial interaction between the polymer and CNTs. In particular, the concentration of CNTs in the composite fibers and the specific interfacial interaction based on the chemical functionalization of the CNTs are the most critical factors in the initial stage because they can strongly influence the physical properties of the final composite fibers [32]. Furthermore, increasing the CNT content in the composite fibers may be advantageous and more desirable for high electrical and thermal properties, as well as for outstanding mechanical performances.

To delve into the influences of the chemical functionalization of CNTs on the structure-property relationship of polymer composite fibers with a high CNT content (~20 wt%), in the present study, a series of elastomeric copolyetherester (CPEE)-based composite fibers containing various neat and functionalized multi-walled carbon nanotubes (MWCNTs) were manufactured using a conventional wet-spinning and coagulation process. The effects of chemically functionalized MWCNTs on the morphological feature, thermal transition, tensile mechanical performance, interfacial interaction, and electrical conductivity of CPEE/MWCNT composite fibers were investigated using scanning electron microscopy, differential scanning calorimetry, a universal tensile test, Raman spectroscopy, and a multimeter.

Experimental

Materials

Pristine MWCNTs (p-MWCNT, diameter of 10-15 nm, length of 10-20 μm, and purity of ~95 %) manufactured through a CVD process were supplied from Hanwha Nanotech, Co. (Republic of Korea). Nitric acid (60-61 %) and sulfuric acid (95 %) for the acid treatment of the MWCNTs were purchased from Samchun Chemical, Co. Ethylene glycol (EG) and Poly(ethylene glycol) (PEG, $\overline{M}_n$ of ~600 g/mol) for the surface modification of the MWCNTs were also obtained from Samchun Chemical, Co. Dimethyl terephthalate (DMT), 1,4-butanediol (1,4-BD), and poly (tetramethylene glycol) (PTMG, $\overline{M}_n$ of ~2000 g/mol) as the monomers for a segmented block copolyetherester (CPEE) elastomer were purchased from SK Chemicals and BASF, Co., respectively. Titanium butoxide was used as the catalyst for synthesizing the CPEE. In addition, 1,1,2,2-tetrachloroethane (TCE), phenol, and methanol for the wet-spinning process were supplied from Samchun Chemical, Co. All chemicals and reagents were used as purchased without further purification.

Synthesis of Polyester Elastomer

A two-step polymerization process was conducted using a lab-scale polymerization reactor for the CPEE elastomer. The first step was a transesterification of the DMT with 1,4-BD and PTMG, and the second step was a polycondensation reaction using the CPEE oligomer obtained during the first step. The transesterification time was controlled based on the amount of distilled methanol, and excess 1,4-BD was collected as a by-product during the polycondensation reaction. At the end of the polycondensation, the final product was extruded as a strand into a cooling water bath using the pressure of nitrogen gas. The strand obtained was cut into chips. The synthesized CPEE elastomer has a 50 % hard segment based on the DMT, and the 1,4-BD has a 50 % soft segment based on both the DMT and PTMG.

Preparation of Functionalized MWCNTs

Acid-treated MWCNTs (a-MWCNT) were prepared through an acid-treatment of pristine MWCNTs. Pristine MWCNTs were added to a mixed solution of sulfuric acid and nitric acid (3/1, v/v). The solution was refluxed at 140 °C for 20 min, cooled to room temperature, diluted through the addition of excess deionized water, and then vacuum-filtered through a PTFE membrane with a 0.45-mm pore size. The filtrate was washed with an excess of distilled water until reaching pH 7. The filtrated solid of the a-MWCNTs was dried for 24 hr at 80 °C under a high vacuum.

Ethylene glycol-modified MWCNTs (MWCNT-EG) and poly(ethylene glycol)-modified MWCNTs (MWCNT-PEG) were prepared by reacting a-MWCNTs with aqueous EG and PEG, respectively. First, the mixture of a-MWCNTs with EG or PEG was sonicated for 5 hr and then added into the reactor. An esterification reaction was then carried out for 8 hr at 200 °C with mechanical stirring at 100 rpm. Water as a by-product was distillated during the reaction. After the

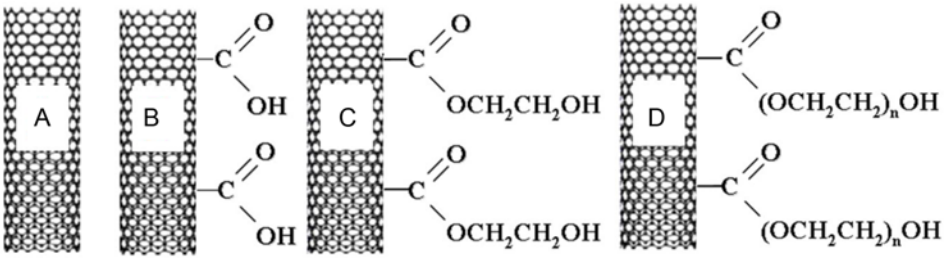

Figure 1. Schematic illustration of MWCNTs used in this study; (A) pristine MWCNT, (B) acid-modified MWCNT, (C) EG-modified MWCNT, and (D) PEG-modified MWCNT.

esterification reaction, the mixture was filtrated through PTFE membranes with a 0.45 mm pore size. The filtrated MWCNT-EGs and MWCNT-PEGs were dried for 25 hr at 80 °C under a high vacuum. A schematic illustration of the pristine MWCNTs and functionalized MWCNTs is shown in Figure 1.

Preparation of Composite Fibers

A predetermined amount of p-MWCNTs and functionalized MWCNTs was added to a phenol/TCE solution and sonicated using a horn-type sonicator (Sonic Dismembrator Model 500, Fisher Scientific, Inc.). Next, neat CPEE was added into the MWCNT solutions and mixed for 3 hr with mechanical stirring. MWCNT contents were controlled to ~20 wt% in the final composite fibers, excluding each of the functionalized groups, and confirmed to be 20.7 wt% of p-MWCNT, 22.9 wt% of a-MWCNT, 26.2 wt% of MWCNT-EG and 24.8 wt% of MWCNT-PEG in the composite fibers. CPEE/MWCNT composite fibers were prepared using a wet-spinning apparatus, which consists of a syringe pump, coagulation bath, and rotating stage. The coagulation baths were kept at 2 °C. Continuous fiber spinning was achieved by controlling the extrusion rate, take-up speed, and concentration of the spinning solution. All of the composite fibers were dried in a vacuum oven at 30 °C for three days.

Characterization of Composite Fibers

The morphological features of various functionalized MWCNTs and their composite fibers were characterized using field emission scanning electron microscopy (FE-SEM, JEOL, JSM-7000F). X-ray photoelectron spectroscopy (XPS, ESCA 2000, MultiLab) was also applied to investigate the surface chemical structures of the functionalized MWCNTs. TGA thermograms were obtained using a TGA-7 (Perkin Elmer) at 30 to 800 °C with a heating rate of 20 °C/min under a nitrogen atmosphere. The thermal properties of the composite fibers were measured using a differential scanning calorimeter (DSC 2910, TA Instruments) over a temperature range of 30-240 °C at a heating rate of 20 °C/min. The non-isothermal crystallization kinetics of the composite fibers were investigated by cooling the samples from 240 °C to 30 °C at various cooling rates. The crystal structures of the various composite fibers were characterized using a wide-angle X-ray diffraction method (M18XHF X-ray diffractometer, MAC Science). The interfacial interaction between the MWCNTs and CPEE matrix in the composite fibers was evaluated using Raman spectroscopy (Renishaws, inVia Raman microscope, RM 1000). The tensile mechanical properties of the composite fibers were measured using a universal tensile machine (Instron model 4467) at a crosshead speed of 2 mm/min. Ten measurements for each composite fiber type were carried out, and the resulting mechanical data were averaged. The electrical conductivities of the composite fibers were evaluated using a multimeter (Fluke 45 Dual Display Multimeter, with a Yokogawa 2552 DC voltage current standard) with a four-probe method.

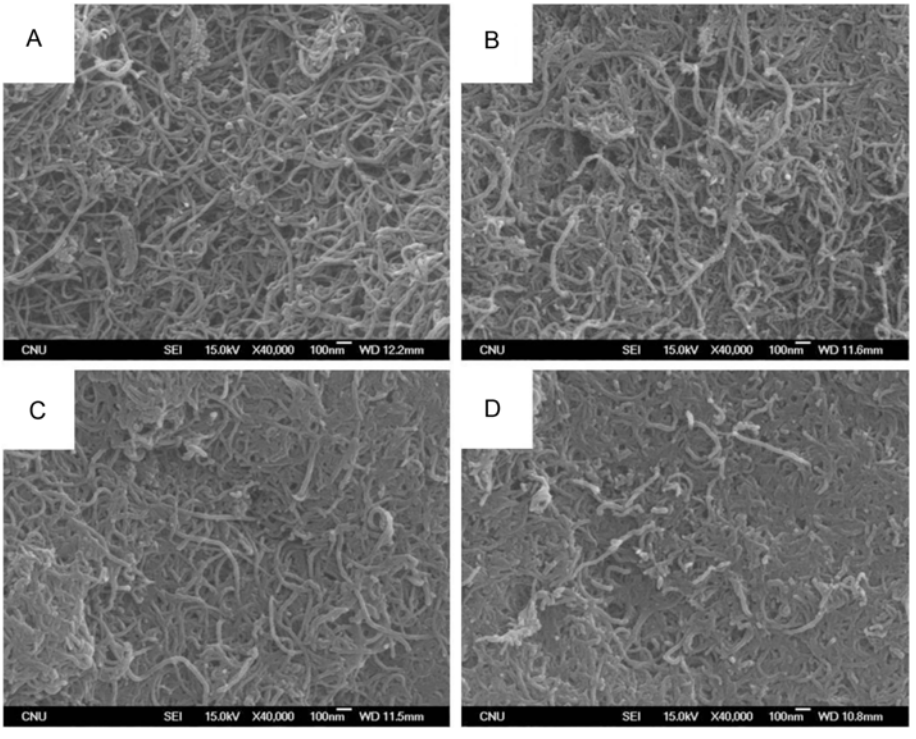

Figure 2. FE-SEM images of (A) pristine MWCNTs, (B) acid-modified MWCNTs, (C) EG-modified MWCNTs, and (D) PEG-modified MWCNTs.

Results and Discussion

Characterization of Functionalized MWCNTs

FE-SEM images of the various functionalized MWCNTs used in this study are shown in Figure 2. The average diameters of the p-MWCNTs (Figure 2(A)) and a-MWCNTs (Figure 2(B)) were measured to be within the range of 10 to 20 nm, whereas the average diameters of the MWCNT-EGs (Figure 2(C)) and MWCNT-PEGs (Figure 2(D)) were evaluated to be within the range of 20 to 30 nm and 30 to 50 nm, respectively. In particular, the large increase in the average diameter of the MWCNT-PEGs compared with the other MWCNTs is believed to be due to the existence of PEG chains on the MWCNT surface. To confirm the chemical functionalization of the MWCNTs, the XPS spectra of the p-MWCNTs, a-MWCNTs, MWCNT-EGs, and MWCNT-PEGs were obtained, as can be seen in Figure 3. For all of the MWCNTs, a common dominant peak is detected at 284.6 eV, which corresponds to the C_{1s} graphitic carbons associated with the sp^2 C=C and sp^3 C-C bonds. Other peaks at 285.8, 286.8, and 288.5 eV observed for the functionalized MWCNTs are assigned to the C-O, C=O, and COO carbons bonds, respectively. The XPS spectrum of the p-MWCNTs displayed relatively weak C=O and COO bonding, as shown in Figure 3(A). On the other hand, the XPS spectra of the a-MWCNTs exhibited a more intense C=O bonding (Figure 3(B)), which originated from the carboxylic acid groups covalently attached to the MWCNTs from the acid treatment. For the MWCNT-EGs (Figure 3(C)) and MWCNT-PEGs (Figure 3(D)), the intensity of the carbon peak at 285.8 eV, which is related with the C-O bond, is strongly increased compared to that of the a-MWCNTs, which stems from the EG and PEG molecules bonded covalently to the MWCNTs through an esterification reaction [33,34]. In addition, the difference in the peak intensity of the C-O bonding between the MWCNT-EGs and MWCNT-PEGs is explained by the large number of ether linkages (C-O-C) existing within the PEG molecules in the MWCNT-PEGs. Therefore, it seems reasonable to conclude that the carboxylic acid groups, EG molecules, and PEG molecules were successfully bonded to the MWCNTs through the acid treatment and esterification reaction.

To evaluate the relative amount of functional groups on the MWCNTs, TGA thermograms of the p-MWCNTs, a-MWCNTs, MWCNT-EGs, and MWCNT-PEGs were obtained, as shown in Figure 4. For the p-MWCNTs, no noticeable weight loss was detected over the temperature range of 30-600 °C. On the other hand, the a-MWCNTs showed a slow weight loss over this temperature range owing to the release of volatile molecules generated from the carboxylic acids or hydroxyl groups, and had a residue of 88.3 wt% at 600 °C. The overall decomposition behaviors of the MWCNT-EGs and MWCNT-PEGs were quite similar, except for the residue at 600 °C. In particular, the weight losses of the MWCNT-

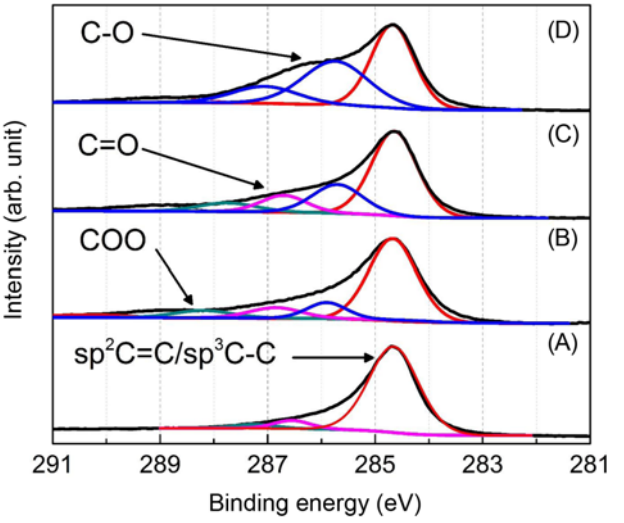

Figure 3. XPS C_{1s} spectra obtained from (A) pristine MWCNTs, (B) acid-modified MWCNTs, (C) EG-modified MWCNTs, and (D) PEG-modified MWCNTs.

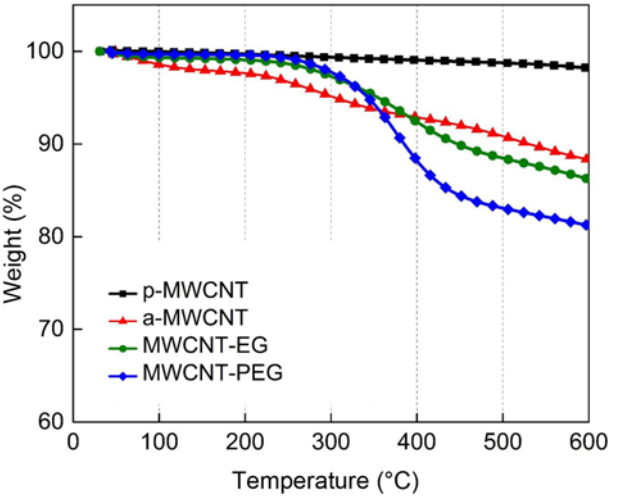

Figure 4. TGA thermograms of neat and functionalized MWCNTs used in this study.

EGs and MWCNT-PEGs were substantially progressed within a temperature range of 250-450 °C, which is due to the thermal degradation of the EG and PEG molecules attached to the MWCNTs. For both the MWCNT-EGs and MWCNT-PEGs, the residue at 600 °C was measured to be 86.2 and 81.2 wt%, respectively. These TGA results are consistent with the SEM images and XPS analyses.

Morphological Characterization of Composite Fibers

The functional groups attached to the MWCNTs are considered to be one of the crucial parameters significantly influencing the dispersibility of MWCNTs in an aqueous spinning solution, the spinnability during the wet-spinning

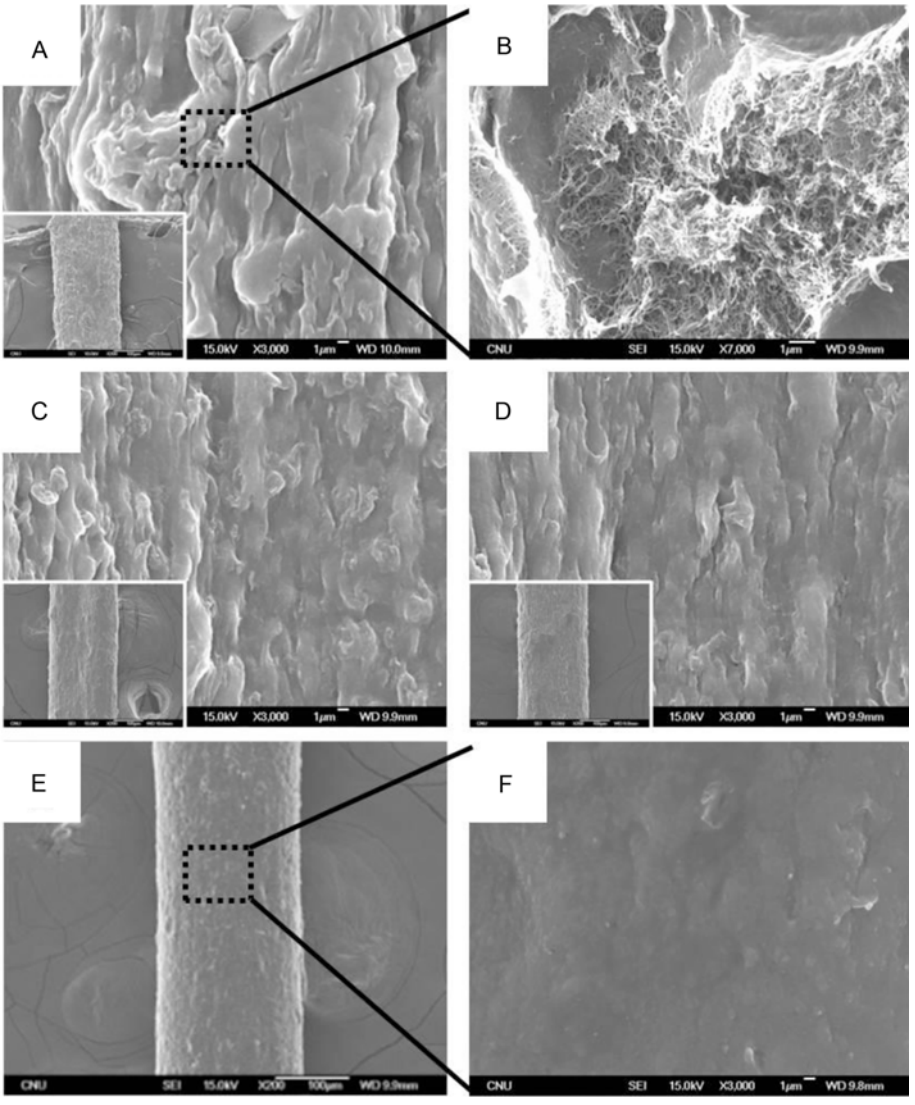

Figure 5. FE-SEM images of (A, B) CPEE/p-MWCNT, (C) CPEE/a-MWCNT, (D) CPEE/MWCNT-EG, and (E, F) CPEE/MWCNT-PEG composite fibers.

process, and the physical properties of the final composite fibers. To examine the morphology of the composite fibers according to the functional groups attached to the MWCNTs, FE-SEM images of various composite fibers prepared using the wet-spinning process are shown in Figure 5. The average diameters of all composite fibers were measured to be within the range of 180-200 μm. However, it was found that the surface morphologies of the composite fibers differ significantly according to the MWCNTs used. In particular, the CPEE/p-MWCNT composite fibers have a very rough surface morphology (Figure 5(A)), which may be related to the MWCNT aggregates in the composite fibers (Figure 5(B)). Thus, it is believed that the MWCNT aggregates in the composite fibers are caused by a poor compatibility between the MWCNTs and CPEE matrix, as well as by the van der Waals interaction among the MWCNTs. Although the CPEE/a-MWCNT (Figure 5(C)) and CPEE/MWCNT-EG (Figure 5(D)) composite fibers displayed relatively smooth surface morphologies compared with the CPEE/p-MWCNT composite fiber, they still had a rough surface topology. On the other hand, the CPEE/MWCNT-PEG composite fiber exhibited a very smooth surface morphology without any noticeable MWCNT aggregates (Figure 5(E), (F)). This result strongly supports the fact that MWCNT-PEGs are well dispersed in the CPEE matrix with improved compatibility and a good interfacial adhesion.

Thermal and Structural Properties of Composite Fibers

Figure 6(A) shows DSC heating thermograms of the CPEE/p-MWCNT, CPEE/a-MWCNT, CPEE/MWCNT-EG,

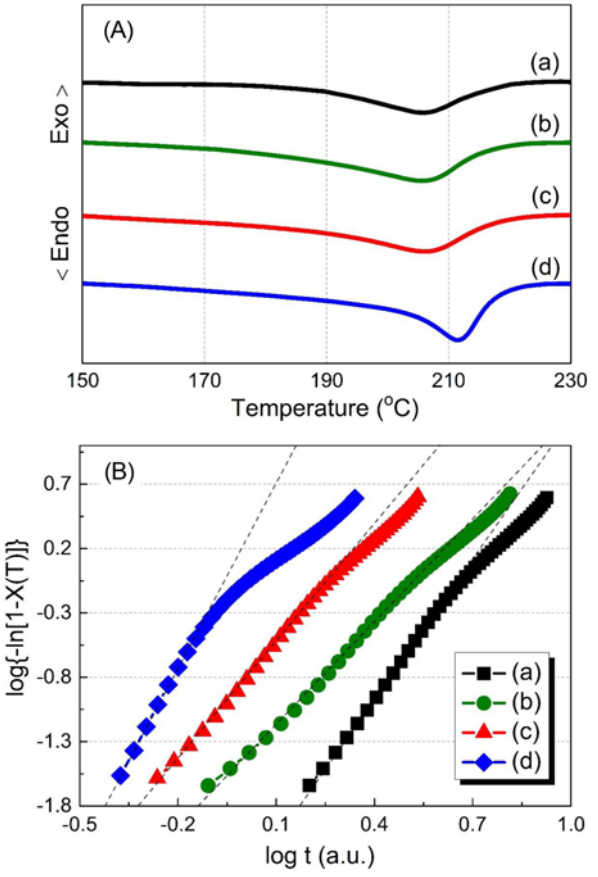

Figure 6. DSC heating thermograms (A) and modified-Avrami plots (B) of CPEE/MWCNT composite fibers; (a) CPEE/p-MWCNT, (b) CPEE/a-MWCNT, (c) CPEE/MWCNT-EG, and (d) CPEE/MWCNT-PEG composite fibers.

and CPEE/MWCNT-PEG composite fibers, the characteristic results of which are summarized in Table 1. Interestingly, it was found that T_m, ΔH_m, and X_c of the CPEE/MWCNT-PEG composite fiber were much higher than those of the other composite fibers. For instance, ΔH_m and X_c of the CPEE/MWCNT-PEG composite fiber were increased by 34.0 % and 33.9 %, respectively, compared to the CPEE/p-MWCNT composite fibers. In addition, T_m of the CPEE/MWCNT-PEG composite fiber is somewhat higher than that of the other composite fibers at up to ~5 °C, which supports the fact that the MWCNT-PEGs may act as an efficient nucleation agent owing to the improved interaction between the CPEE and MWCNT-PEGs.

To confirm the effects of functionalized MWCNTs on the crystallization behaviors of the various composite fibers, the non-isothermal crystallization kinetics was investigated using DSC measurements. The most common approach used to compare the non-isothermal crystallization kinetics is the Avrami equation [35,36], which assumed that the relative crystallinity, $X(t)$ developed with crystallization time t,

Table 1. Thermal properties and Avrami exponent (n) of CPEE/MWCNT composite fibers from DSC heating and non-isothermal crystallization experiment

Sample code	T_m (°C)	ΔH_m (J/g)	X_c (%)	Avrami exponent, n
CPEE/p-MWCNT	205.1	16.0	22.7	3.5
CPEE/a-MWCNT	206.4	19.1	27.1	2.8
CPEE/MWCNT-EG	206.7	18.4	26.1	3.0
CPEE/MWCNT-PEG	210.9	25.6	36.3	4.6

$$1 - X(t) = \exp(Zt^n) \quad (1)$$

where Z is the composite crystallization rate constant, and n is the Avrami exponent. It should be mentioned that although the Z and n parameters do not have the same physical meaning because the temperature changes instantly in the non-isothermal crystallization, the use of equation (1) can provide further insight into the kinetics of non-isothermal crystallization. Jeziorny [37] suggested that the value of rate parameter Z should be adequately corrected. The factor that should be considered was the cooling rate. Assuming constant or approximately constant, the final form of the parameter characterizing the kinetics of non-isothermal crystallization was given as:

$$\log Z_c = \frac{\log Z}{\phi} \quad (2)$$

Figure 6(B) shows the modified-Avrami plots obtained from the non-isothermal crystallization experiments at various cooling rates. It was found that the slopes of the plots differ somewhat, which indicates the various crystallization mechanisms of the composite fibers owing to the surface modification of the MWCNTs. The linear portion during the initial step of the modified-Avrami plot is typically considered to be due to the primary crystallization. Accordingly, the Avrami exponent n of all composite fibers was determined from the slope of the initial portion, which is summarized in Table 1. The Avrami exponent n of the CPEE/p-MWCNT, CPEE/a-MWCNT, and CPEE/MWCNT-EG composite fibers was evaluated to be 3.2, 2.8, and 3.0, respectively, and there were no major differences among these composite fibers, as listed in Table 1. On the other hand, the Avrami exponent n of the CPEE/MWCNT-PEG composite fiber is much higher than that of the other composite fibers, indicating that the crystal growth occurs at a higher dimension than in the other composite fibers, and that the MWCNT-PEGs in the composite fiber serve as an efficient nucleating agent for the CPEE matrix. Overall, it is believed that the introduction of MWCNTs containing sufficiently long, flexible chains effectively facilitates the crystallization and effective nucleating capability of the MWCNTs, eventually leading to the enhanced thermal properties of the composite fibers.

Because the thermal properties and crystallization behaviors

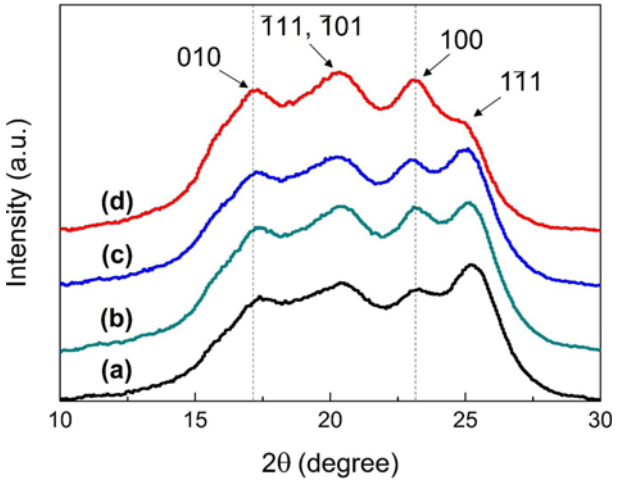

Figure 7. WAXD patterns of CPEE/MWCNT composite fibers; (a) CPEE/p-MWCNT, (b) CPEE/a-MWCNT, (c) CPEE/MWCNT-EG, and (d) CPEE/MWCNT-PEG composite fibers.

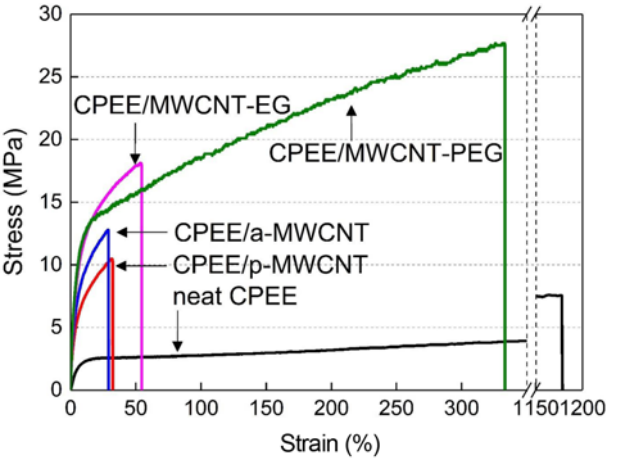

Figure 8. Stress-strain curves of CPEE/MWCNT composite fibers.

of the composite fibers are strongly affected by the functional groups on the MWCNTs, it is thought that the existence of functionalized MWCNTs in the composite fibers has a significant influence on the crystal growth of the CPEE matrix. Figure 7 shows the WAXD patterns of various composite fibers. As can be seen in Figure 8, similar reflection peaks were observed at 2θ=17.3, 20.5, 23.1, and 25.0°, which are assigned to be 010, $\bar{1}11$/$\bar{1}01$, 100, and $1\bar{1}1$, respectively, in the α-form of poly(butylene terephthalate), which corresponds to the hard segment of the CPEE matrix [38]. Nonetheless, for the CPEE/MWCNT-PEG composite fiber, intensities of 010 and 100 reflections are much higher than those of other composite fibers, except for the $1\bar{1}1$ reflection, indicating that the CPEE crystals in the composite fiber were relatively well-developed and aligned along the fiber axis. In addition, this result suggests that the well-developed crystals are due to the templating effect of the MWCNTs embedded along the composite fiber axis. Therefore, it is valid to state that, despite the relatively high content of MWCNTs used in this study, the sufficiently long and flexible PEG chains on the MWCNTs improve the crystal growth of the CPEE matrix owing to the nucleation effect of the MWCNTs.

Mechanical Properties of Composite Fibers

Tensile mechanical tests of various composite fibers were carried out, as shown in Figure 8, the results of which are summarized in Table 2. It was found that the tensile mechanical properties of the composite fibers containing various functionalized MWCNTs are much higher than those of the CPEE/p-MWCNT composite fiber. For instance, the initial modulus and tensile strength of the CPEE/a-MWCNT composite fiber were evaluated to be 0.26 GPa and 12.7 MPa, respectively, and for the CPEE/MWCNT-EG composite fiber, the initial modulus and tensile strength were measured to be 0.32 GPa and 18.0 MPa. Furthermore, it is very interesting to note that the initial modulus and tensile strength of the CPEE/MWCNT-PEG composite fiber were increased noticeably by 380 % and 162 %, respectively, compared to the CPEE/p-MWCNT composite fibers. In addition, the breaking strain of the CPEE/MWCNT-PEG composite fiber was measured to be 330 %, as compared to the 28-54 % breaking strain of the other composite fiber types, which indicates that an efficient stress transfer occurs even at a higher strain region owing to the good interfacial interaction between the CPEE matrix and the MWCNT-PEGs.

Table 2. Tensile mechanical properties and MWCNTs alignment of CPEE/MWCNT composite fibers

Sample code	Initial modulus (GPa)	Tensile strength (MPa)	Breaking strain (%)	MWCNTs alignment (*A*)[a]
CPEE/p-MWCNT	0.10	10.5	32.8	0.36
CPEE/a-MWCNT	0.26	12.7	28.9	0.35
CPEE/MWCNT-EG	0.32	18.0	54.3	0.27
CPEE/MWCNT-PEG	0.48	27.5	333.2	0.30

[a]MWCNTs alignment were relatively evaluated based on the polarized Raman analysis [41] and [b]for neat CPEE fiber, initial modulus, tensile strength and breaking strain were measured to be 0.03 GPa, 7.54 MPa and 1,177.9 %, respectively.

The efficiency of the stress transfer from the CPEE matrix to the functionalized MWCNTs for various composite fibers can be characterized using a Raman shift of the D* band of the MWCNTs under a tensile deformation [39,40]. The strain-dependent Raman shifts of the D* bands for all composite fiber types are shown in Figure 9(A). It was observed that the position of the D* band changes to a lower wavenumber with an increase in the applied strain. In particular, the initial change of the D* band of the CPEE/

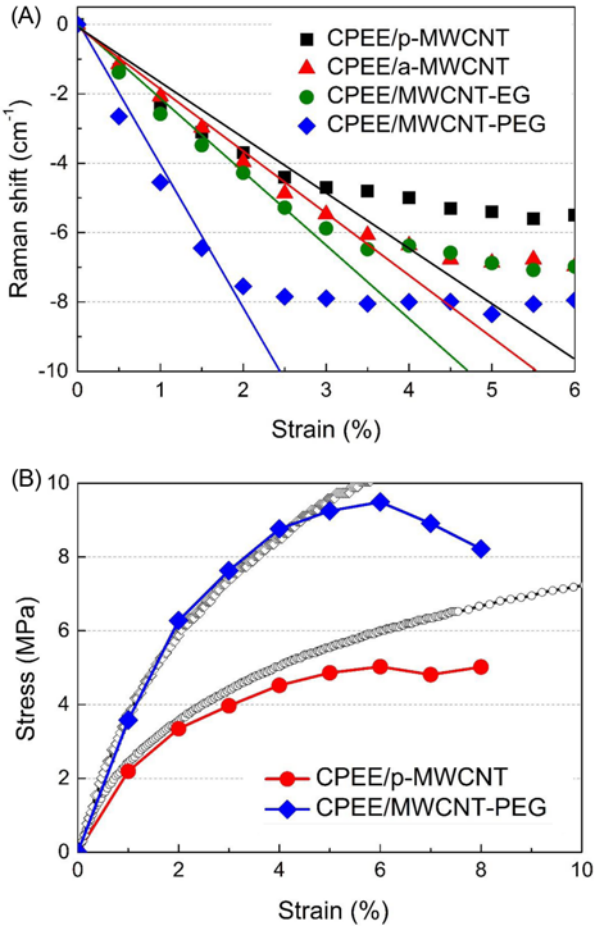

Figure 9. (A) Strain-induced D* band shifts for CPEE/MWCNT composite fibers and (B) experimental (empty symbol) and calculated (solid line, symbols) stress-strain curves of the composite fibers.

MWCNT-PEG composite fiber on the applied strain was mostly steeper than that of the other composite fibers, which suggests that the stress transfer takes places most efficiently in the CPEE/MWCNT-PEG composite fiber. Considering that the tensile mechanical properties of polymer/CNT composite systems are associated with the change in Raman shift on the applied strain, this can also be understood by correlating the strain-dependent Raman shift with the tensile deformation behavior. In Figure 9(B), experimental stress-strain curves (empty symbol) of two composite fibers are compared with the calculated values (solid line, symbol) according to the shifts in the Raman position. It was observed that, for the CPEE/MWCNT-PEG composite fiber, the calculated data are quite consistent with the experimental values at up to a ~5 % strain level, as well as with the stress values, when compared to the CPEE/p-MWCNT composite fiber. As listed in Table 2, because the difference in MWCNT alignment among all of the composite fibers is negligible, the Raman shift results indicate that the highly improved

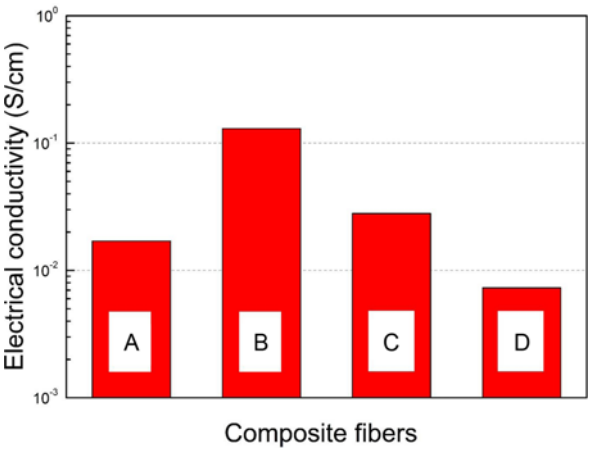

Figure 10. Electrical conductivities of (A) CPEE/p-MWCNT, (B) CPEE/a-MWCNT, (C) CPEE/MWCNT-EG, and (D) CPEE/MWCNT-PEG composite fibers.

initial modulus of the CPEE/MWCNT-PEG composite fiber originates from the enhanced interfacial interaction between the MWCNT-PEGs and CPEE matrix, eventually leading to an effective stress transfer for the composite fibers. This result is also consistent with the FE-SEM, DSC, and WAXS results described above.

Electrical Properties of Composite Fibers

To investigate the effect of functionalized MWCNTs on the electrical properties of various composite fibers, the electrical conductivities of the composite fibers were characterized, as shown in Figure 10. The electrical conductivity of CPEE/a-MWCNT composite fiber was measured to be ~1.3×10^{-1} S/cm, which was the highest among the composite fibers studied. The electrical conductivities of the CPEE/p-MWCNT and CPEE/MWCNT-EG composite fibers were also evaluated to be 1.7×10^{-2} and 2.8×10^{-2} S/cm, respectively. It is believed that the enhanced electrical conductivity of the CPEE/a-MWCNT composite fiber may originate from the formation of an efficient electrical conduction path through direct contact among the a-MWCNTs in the composite fibers. On the other hand, for the CPEE/MWCNT-PEG composite fiber, the electrical conductivity was relatively lower than that of the other composite fibers. This result can be explained by the fact that, although the MWCNT-PEGs are well-dispersed throughout the composite fibers, the MWCNTs are well-covered with PEG chains and form a physical entanglement with the CPEE chains, which serve as physical barriers by preventing the formation of an efficient electrical conduction path among the neighboring MWCNTs within the composite fibers [41].

Conclusion

Different types of CPEE-based composites fibers containing

various neat or functionalized MWCNTs were manufactured using a conventional wet-spinning and coagulation process. It was shown through FE-SEM images that the CPEE/MWCNT-PEG composite fiber has a smooth surface morphology owing to the good compatibility between the MWCNT-PEGs and CPEE matrix, whereas the other composite fibers containing p-MWCNTs, a-MWCNTs, and MWCNT-EGs exhibited a very rough surface morphology owing to the MWCNT aggregates. As a result, thermal characteristics such as T_m, ΔH_m, and X_c of the CPEE/MWCNT-PEG composite fiber were noticeably increased compared to those of the other composite fibers. In addition, the tensile mechanical properties of the CPEE/MWCNT-PEG composite fiber were much higher than those of the other composite fibers, which originate from the efficient stress transfer from the CPEE matrix to the MWCNT-PEGs. The effective stress transfer in the CPEE/MWCNT-PEG composite fiber was confirmed through a Raman spectroscopic analysis, which shows that the Raman band position was highly shifted with the increment of the applied strain. On the other hand, the electrical conductivity of the CPEE/MWCNT-PEG composite fiber was somewhat lower than that of the other composite fiber types including the p-MWCNT, a-MWCNT, and MWCNT-EG fibers. This result is explained by the fact that, in the case of the CPEE/MWCNT-PEG composite fiber, the MWCNTs were well covered with PEG chains, which eventually resulted in preventing the formation of an efficient electrical conduction path among the MWCNTs in the composite fibers. Overall, it can be concluded that the introduction of sufficiently long and flexible PEG chains on the MWCNTs contributed to enhancing the interfacial interactions between the MWCNTs and CPEE matrix, as well as to the nucleating capability of the MWCNTs on the crystallization of the CPEE, eventually leading to the improved thermal and mechanical properties of the CPEE-based composite fiber.

References

1. S. J. Tans, M. H. Devoret, H. Dai, A. Thess, R. E. Smalley, L. Georliga, and C. Dekker, *Nature*, **386**, 474 (1997).
2. S. D. Lee, O. J. Kwon, B. C. Chun, J. W. Cho, and J. S. Park, *Fiber. Polym.*, **10**, 71 (2009).
3. D. Walters, L. Ericson, M. Casavant, J. Liu, D. Colbert, K. Smith, and R. Smalley, *Appl. Phys. Lett.*, **74**, 3803 (1999).
4. M. H. Jee, J. S. Lee, J. Y. Lee, Y. G. Jeong, and D. H. Baik, *Fiber. Polym.*, **11**, 1 (2010).
5. H. J. Jang, W. J. Kim, and Y. S. Chung, *Text. Sci. Eng.*, **53**, 24 (2016).
6. R. H. Baughman, A. A. Zakhidov, and W. A. de Heer, *Science*, **297**, 787 (2002).
7. M. F. Yu, B. S. Files, S. Arepalli, and R. S. Ruoff, *Phys. Rev. Lett.*, **84**, 5552 (2000).
8. H. H. No, G. Yuang, D. H. Cho, and J. K. Lee, *Text. Sci. Eng.*, **53**, 171 (2016).
9. N. Behabtu, M. J. Green, and M. Pasquali, *Nano Today*, **3**, 24 (2008).
10. M. J. Green, N. Behabtu, M. Pasquali, and W. W. Adams, *Polymer*, **50**, 4979 (2009).
11. W. K. Choi, G. Y. Park, H. S. Shin, Y. S. Kuk, B. S. Kim, and M. K. Seo, *Text. Sci. Eng.*, **54**, 209 (2017).
12. H. G. Chae and S. Kumar, *Science*, **319**, 908 (2008).
13. F. Mai, D. Pan, X. Gao, M. Yao, H. Deng, K. Wang, F. Chen, and Q. Fu, *Polym. Int.*, **60**, 1646 (2011).
14. X. Xu, A. J. Uddin, K. Aoki, Y. Gotoh, T. Saito, and M. Yumura, *Carbon*, **48**, 1977 (2010).
15. L. Deng, R. J. Young, S. van der Zwaag, and S. Picken, *Polymer*, **51**, 2033 (2010).
16. J. M. Razal, J. N. Coleman, E. Munoz, B. Lund, Y. Gogotsi, H. Ye, S. Collins, A. B. Dalton, and R. H. Baughman, *Adv. Func. Mater.*, **17**, 2918 (2007).
17. E. Muñoz, D. S. Suh, S. Collins, M. Selvidge, A. B. Dalton, B. G. Kim, J. M. Razal, G. Ussery, A. G. Rinzler, and M. T. Martínez, *Adv. Mater.*, **17**, 1064 (2005).
18. E. Munoz, A. B. Dalton, S. Collins, M. Kozlov, J. Razal, J. N. Coleman, B. G. Kim, V. H. Ebron, M. Selvidge, and J. P. Ferraris, *Adv. Eng. Mater.*, **6**, 801 (2004).
19. S. Ruan, P. Gao, and T. Yu, *Polymer*, **47**, 1604 (2006).
20. Z. Li, G. Luo, F. Wei, and Y. Huang, *Compos. Sci. Technol.*, **66**, 1022 (2006).
21. Q. Meng and J. Hu, *Compos. Part A: Appl. Sci. Manuf.*, **39**, 314 (2008).
22. L. Shen, X. Gao, Y. Tong, A. Yeh, R. Li, and D. Wu, *J. Appl. Polym. Sci.*, **108**, 2865 (2008).
23. S. Kumar, T. D. Dang, F. E. Arnold, A. R. Bhattacharyya, B. G. Min, X. Zhang, R. A. Vaia, C. Park, W. W. Adams, and R. H. Hauge, *Macromolecules*, **35**, 9039 (2002).
24. B. G. Min, T. Sreekumar, T. Uchida, and S. Kumar, *Carbon*, **43**, 599 (2005).
25. H. G. Chae, M. L. Minus, A. Rasheed, and S. Kumar, *Polymer*, **48**, 3781 (2007).
26. B. Vigolo, A. Penicaud, C. Coulon, C. Sauder, R. Pailler, C. Journet, P. Bernier, and P. Poulin, *Science*, **290**, 1331 (2000).
27. B. Vigolo, P. Poulin, M. Lucas, P. Launois, and P. Bernier, *Appl. Phys. Lett.*, **81**, 1210 (2002).
28. P. Miaudet, S. Badaire, M. Maugey, A. Derre, V. Pichot, P. Launois, P. Poulin, and C. Zakri, *Nano Lett.*, **5**, 2212 (2005).
29. A. B. Dalton, S. Collins, J. Razal, E. Munoz, V. H. Ebron, B. G. Kim, J. N. Coleman, J. P. Ferraris and R. H. Baughman, *J. Mater. Chem.*, **14**, 1 (2004).
30. M. H. Jee, S. H. Park, J. U. Choi, Y. G. Jeong, and D. H. Baik, *Fiber. Polym.*, **13**, 443 (2012).
31. M. H. Jee, J. U. Choi, S. H. Park, Y. G. Jeong, and D. H. Baik, *Macromol. Res.*, **20**, 650 (2012).
32. N. Lachman, C. Bartholome, P. Miaudet, M. Maugey, P. Poulin, and H. D. Wagner, *J. Phys. Chem. C*, **113**, 4751

(2009).
33. C. Bergeret, J. Cousseau, V. Fernandez, J.-Y. Mevellec, and S. Lefrant, *J. Phys. Chem. C*, **112**, 16411 (2008).
34. K. A. Wepasnick, B. A. Smith, J. L. Bitter, and D. H. Fairbrother, *Anal. Bioanal. Chem.*, **396**, 1003 (2010).
35. G. Liang, J. Xu, and W. Xu, *J. Appl. Polym. Sci.*, **91**, 3054 (2004).
36. Y. Wang, C. Shen, H. Li, Q. Li, and J. Chen, *J. Appl. Polym. Sci.*, **91**, 308 (2004).
37. A. Jeziorny, *Polymer*, **19**, 1142 (1978).
38. D. Baik, M. Lee, B. Jeon, and M. Han, *Text. Sci. Eng.,* **31**, 613 (1994).
39. W. Ma, L. Liu, R. Yang, T. Zhang, Z. Zhang, L. Song, Y. Ren, J. Shen, Z. Niu, and W. Zhou, *Adv. Mater.*, **21**, 603 (2009).
40. M. Mu, S. Osswald, Y. Gogotsi, and K. I. Winey, *Nanotechnology*, **20**, 335703 (2009).
41. S. Zhang, L. Zhu, M. L. Minus, H. G. Chae, S. Jagannathan, C.-P. Wong, J. Kowalik, L. B. Roberson, and S. Kumar, *J. Mater. Sci.*, **43**, 4356 (2008).